Observation of MHD structures in JET temperature profiles

To cite this article: M.F.F. Nave *et al* 1992 *Nucl. Fusion* **32** 825

OBSERVATION OF MHD STRUCTURES IN JET TEMPERATURE PROFILES

M.F.F. NAVE*, A.W. EDWARDS, K. HIRSCH**, M. HUGON,
A. JACCHIA+, E. LAZZARO+, H. SALZMANN++, P. SMEULDERS
JET Joint Undertaking,
Abingdon, Oxfordshire, United Kingdom

ABSTRACT. Flat regions observed in the profiles of the electron temperature measured by LIDAR Thomson scattering provide evidence for the existence of helical magnetohydrodynamic resistive mode structure in JET discharges. Comparison with profiles of the safety factor q, determined from magnetic equilibrium calculations, shows that the most prominent regions are located close to rational values of q. The flat regions are also correlated with perturbations observed with other independent experimental measurements such as soft X-rays, electron cyclotron emission and Mirnov oscillations.

1. INTRODUCTION

In a tokamak, the non-linear stages of tearing modes arising from finite resistivity effects are expected to develop magnetic islands at surfaces where the safety factor q is rational [1, 2]. Theoretical arguments predict that the background axisymmetric profiles of pressure and current could relax locally to a force free configuration with vanishing gradients across the islands [2, 3]. The magnetic islands are considered to be responsible for Mirnov oscillations, and their unstable evolution is related to disruptions [4].

Early experimental evidence for flattenings in the temperature profiles was provided by Thomson scattering techniques, before disruptions in Pulsator [5] and in steady state conditions in Wendelstein VII-A [6]. Island structures were further observed in PLT, Wendelstein VII-A and JIPP-TII using X-ray tomography [4, 7, 8]. Perturbations looking like small humps were also observed in the emission profiles of the bremsstrahlung continuum radiation measured in TJ-I [9].

In JET, the development of soft X-ray (SXR) tomography analysis [10], electron cyclotron emission (ECE) heterodyne measurements and ECE multichannel spectrometry has provided direct proof of the flattening of X-ray emission and temperature profiles in events associated with disruptions and partial sawteeth. Island structures and flattening of the profiles were seen, located at q = 1, associated with partial sawteeth [11], and located at q = 2, associated with events preceding a disruption [10, 12–14].

More recently, the electron temperature and pressure profiles measured in JET with the new LIDAR Thomson scattering system [15, 16] showed that regions of reduced slope occur very often and can be associated with a variety of magnetohydrodynamic (MHD) activity in non-disruptive conditions [17]. Comparison with the safety factor profiles obtained from the solution of the magnetic equilibrium problem from measured magnetic and diamagnetic signals [18–22] has shown a correlation between the location of low order rational q values and localized flat regions of the electron temperature [17]. Perturbations at the same radial positions are also observed with SXR and ECE diagnostics for the data analysed and are at the same time visible on external magnetic probes. (A review of JET diagnostics is given in Ref. [23].) In JET, magnetic oscillations are observed with frequencies ranging from zero (locked modes) to around 100 kHz. From the analysis of the magnetic data the poloidal and toroidal mode numbers can be determined as well as the location of the O and X points [13]. A wide range of MHD activity is normally observed as a discharge evolves in time, the most important modes being those with low mode numbers: (1, 1), (2, 1) and (3, 2).

Unlike methods of mode analysis requiring line inversion techniques the LIDAR and ECE diagnostics provide a direct local measurement of the profile structure of JET discharges. Here we discuss results obtained with the LIDAR system. The LIDAR system has some

Permanent affiliations:
* Laboratorio Nacional de Engenharia e Tecnologia Industrial, Sacavem, Portugal.
** Institut für Plasmaforschung, Universität Stuttgart, Stuttgart, Germany.
\+ Istituto di Fisica del Plasma, Associazione Euratom-ENEA-CNR, Milan, Italy.
\+\+ Max-Planck-Institut für Plasmaphysik, Garching, Germany.

advantages over conventional Thomson scattering systems in the detection of flat regions since it uses the same set of detectors and thus the same set of calibration constants for measurements at different radii. This eliminates spurious flat regions caused by interspatial channel calibration errors. With the LIDAR system, one effectively takes a snapshot of the temperature profile, with an exposure time of ~7 ns. Since several flat regions (each one associated with a different value of q rational) can be observed simultaneously, the LIDAR profiles may provide an immediate insight into the magnetic topology of the JET plasma. However, since at present the LIDAR profiles have a spatial resolution of 9 cm, we will restrict our analysis to large perturbations that are outside the error bars caused by photon statistics.

We present a data analysis showing the correlation between the LIDAR measurements and the data obtained from several other diagnostics. In Section 2, we discuss examples of individual discharges with electron temperature (T_e) profiles which clearly exhibit flat regions associated with a range of MHD activity with low order poloidal and toroidal mode numbers (m, n). In general, several flat regions are observed simultaneously; however, for the sake of clarity, perturbations related to different mode numbers are discussed separately. In Section 3, we discuss the conditions where smoother LIDAR profiles have been observed. In Section 4, we present the results of a statistical analysis involving 1988 JET discharges which shows the correlation of the temperature profile perturbations with rational q values. Section 5 is a summary, and the Appendix gives details of the LIDAR system and a series of measurements carried out to check for possible spurious profile effects.

2. ANALYSIS OF INDIVIDUAL DISCHARGES EXHIBITING LARGE FLAT REGIONS IN THE TEMPERATURE PROFILES

2.1. General view

LIDAR T_e profiles, measured in the equatorial plane of JET, are in general non-smooth, showing changes of inflection, flat regions and in some cases humps, at several radial positions. Non-smooth temperature profiles are observed under a variety of operational conditions, occurring with both Ohmic and auxiliary heating. The shape of a perturbation is quite often within the experimental error; therefore, in this paper, we will always refer to a perturbation as a 'flat region'. For most of

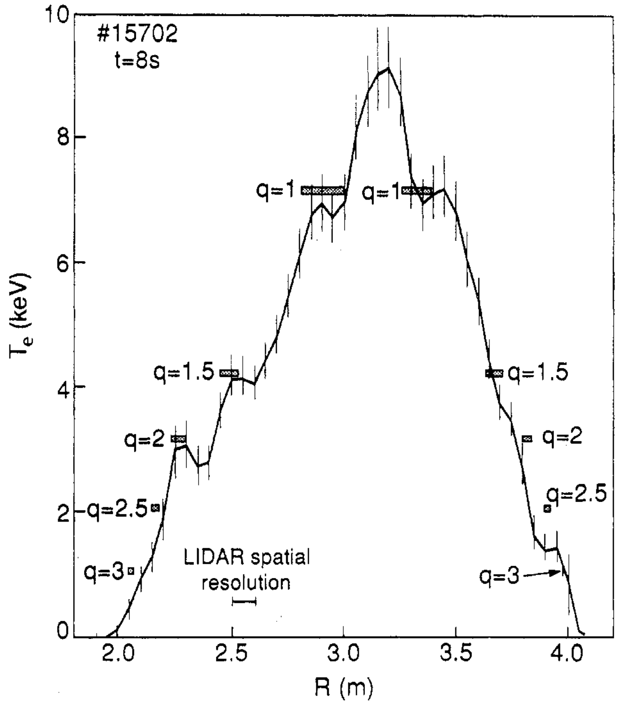

FIG. 1. LIDAR T_e profile showing large perturbations outside the statistical error bars. The boxes indicate the positions of rational q surfaces and their spatial uncertainty.

the large flat regions, i.e. outside the experimental error, a correlation with MHD activity is found, as will be shown in the examples below.

A LIDAR T_e profile which clearly exhibits large perturbations, which cannot be explained by experimental uncertainties, is shown in Fig. 1. The error bars indicate one standard deviation and are due to the photoelectron statistics of the raw LIDAR signals. This profile was taken during ion cyclotron resonance heating (ICRH), 130 ms after a sawtooth crash, when the centre of the plasma has already been reheated. Also shown in the figure are the positions of rational values of q.

The q profiles in this paper were reconstructed using what is now an established non-linear least squares fit of the externally measured tangential magnetic field distribution, under the constraint of satisfying the equilibrium Grad–Shafranov equation with the additional enforcing of the diamagnetic measurement [19]. This technique has been repeatedly tested on given calculated and experimental equilibria [18–21] to establish its space resolution and its response to perturbations of the signals to alternative choices of the parametrized functional form for the toroidal current density $J_\phi(R, \Psi)$. The results of many sensitivity studies now published [20, 21] indicate that the resolution afforded by the magnetic (and diamagnetic)

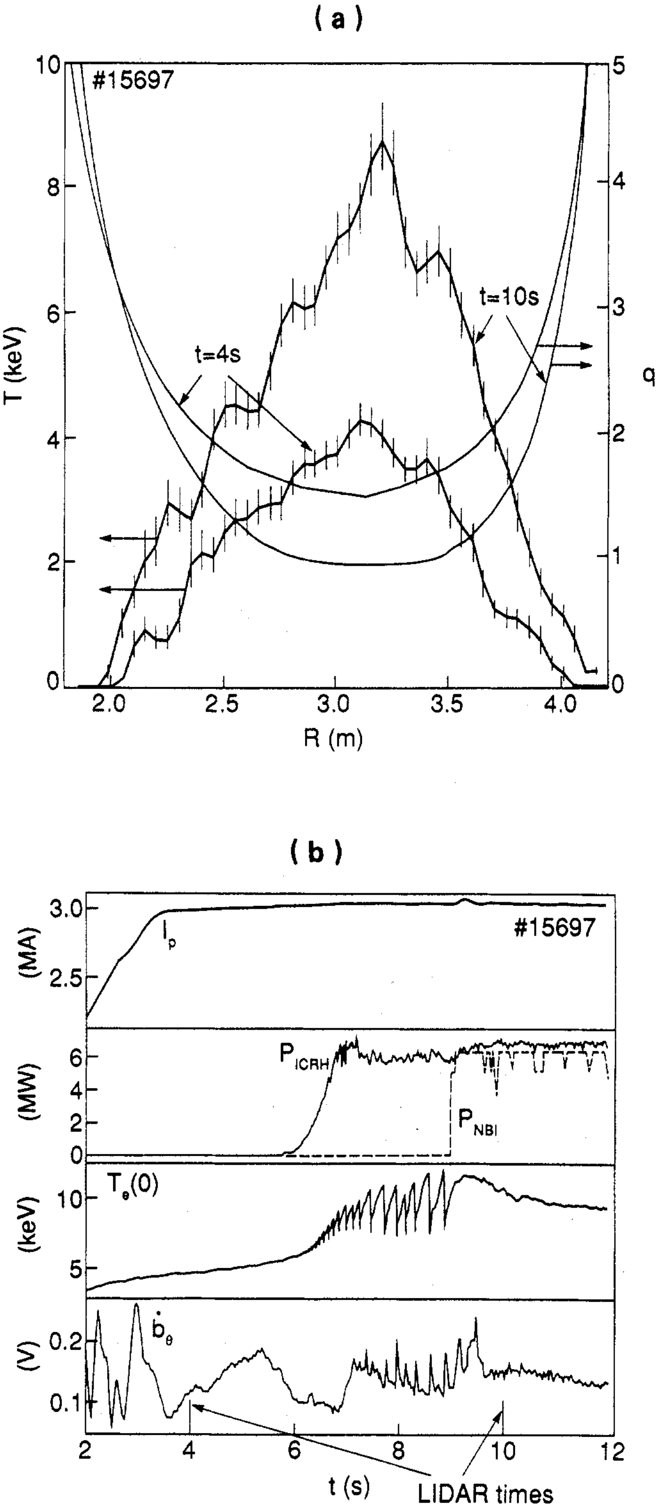

FIG. 2. Observations at different times as a discharge evolves through the current flat-top. (a) T_e and magnetically identified q profiles. (b) Time behaviour of plasma parameters: total plasma current, auxiliary heating power, central temperature, and time derivative of the perturbed poloidal magnetic field (from an $n = 1$ combination of pick-up coil signals measured at 45° above the midplane on the lower field side).

measurements alone leads to an uncertainty of $\pm 15\%$ for the central value of q in the low β discharges considered in this paper. Further inclusion of diagnostic information with potentially higher space resolution, such as multichannel polarimetric measurements and LIDAR pressure profiles (not included here), have modified the reconstructed value of q(0) just within the $\pm 15\%$ bounds. In Refs [19, 20, 22] it is shown that the variation of the functional form of $J_\phi(R, \Psi)$ within a non-pathological class of square integrable functions, vanishing at the plasma boundary, affects the determination of the q profile by less than the response to errors in the measurements and therefore is not a serious cause of error.

Figure 1 indicates a correlation between the calculated positions of rational values of q and the positions of the observed flat regions. The error of $\pm 15\%$ in the centre leads to a variation of the $q = 1$ radius of ± 10 cm. This is combined with an uncertainty of 3 cm on the absolute position of the LIDAR profile, and a spatial resolution of 9 cm due to the response time of the detection system and the laser pulse length. The statistical analysis discussed later confirms the above correlation and also ECE data show the existence of a large flat region around the sawtooth inversion radius, coinciding in position with the central flat region in the LIDAR profile, while the magnetic pick-up coils indicate the presence of rotating $n = 1$ and $n = 2$ modes.

The LIDAR profiles are currently available only at intervals of >1 s and therefore it is not possible to study in detail the evolution in time of the size of the T_e plateaus, except in the special cases of locked modes which can last up to several seconds. The following example shows that the nature of the MHD activity associated with the flat regions may change as the discharge evolves in time.

Figure 2(a) shows the T_e and q profiles obtained at two different times and operational regimes for the same discharge. Information about the discharge and the magnetic perturbation measurements is shown in Fig. 2(b). One profile in Fig. 2(a) with the higher central q value has been taken at the beginning of the current flat-top during the Ohmic heating (OH) phase. The other profile has been measured during the additionally heated phase in the discharge. One can see a modest movement of the $q = 2$ surface by 10 cm on the high field side, from 2.4 to 2.3 m, between these times; a corresponding displacement of the flat region in the LIDAR profile close to this surface is observed.

Figure 2(b) shows that the T_e profile at $t = 4$ s was taken before the appearance of sawteeth in the Ohmic regime. The T_e profile at $t = 10$ s was measured at the beginning of a 'monster sawtooth', i.e. a sawtooth free period followed by a large sawtooth collapse [24], which started when combined neutral beam injection (NBI) heating and ICRH was applied. In this particular case, the amplitude of the n = 1 activity is five to ten times larger than is normally observed during a 'monster sawtooth'. (Sawtooth free periods will be discussed further in Section 3.)

Analysis of the magnetic pick-up coil data shows the presence of two n = 1 modes, one with the frequency of the plasma central rotation (a broad spectrum does not allow for an unambiguous identification of the poloidal number) and an edge mode with a lower frequency identified as an m = 4 mode . The ECE data, just before the sawtooth free period, show a sawtooth inversion radial position of 3.45 m, in agreement with the calculated q = 1 position and the location of the central perturbation observed in the T_e profile.

In the previous examples, the central flattenings associated with the m = 1, n = 1 modes are seen on both sides of the profiles. It is not always possible to distinguish between the effects of an island and a partial sawtooth crash leaving behind a symmetric ring of flat temperatures [11]. However, often only one central m = 1 structure is observed, which changes sides as the mode rotates, as will be shown below.

These examples also show that the perturbations are wider on the inside of the profiles, i.e. on the high field side. This is generally observed and is consistent with predictions of tearing mode theory in toroidal geometry [26, 27]. Numerical simulations with the fixed boundary resistive stability FAR code [28] show that for the m = 2, n = 1 mode, a factor of two could be expected between the inside and the outside island widths [27]. Thus, the spatial resolution of the LIDAR system and the orientation of the islands with respect to the measurement may explain why in some profiles (as the profile at t = 10 s in Fig. 2) the perturbations are hardly visible on the low field side and why there is a lack of symmetry for the flat regions around q = 2. Statistical analysis, discussed later, actually shows that in most cases the m = 2 perturbations are observed simultaneously on both sides of the profile.

Owing to the fact that the magnetic lines are packed close together on the outside, because of the Shafranov shift, and owing to the finite spatial resolution of the measurement, an apparent overlap may occur between two adjacent rational surfaces. This can put the region of reduced slope, spatially as well as in absolute temperature, in between the rational surfaces. In addition, the errors in the positions of the temperature profiles and the positions of rational q can cause an apparent lack of isothermality between flat regions with the same mode numbers observed on the inside and the outside. However, plots of T_e versus q, obtained by interpolating q at the same radial positions as the T_e profile, show that isothermality is verified within 10%.

The following examples of rotating and quasi-stationary modes will illustrate further the correlation between the T_e LIDAR profiles and data from other diagnostics.

2.2. Observation of m = 1, n = 1 modes

In JET, SXR and ECE measurements have shown the presence of m = 1, n = 1 islands under various conditions, often coupled to either rotating or locked modes with m ≥ 2, visible on the magnetic signals. These islands are observed after partial sawtooth collapses, and in several cases they seem to decay into an annular region [11]. Sometimes, in auxiliary heated discharges, m = 1, n = 1 structures with the rotation frequency of the central plasma are observed throughout the sawtooth cycle, although they are apparently not involved in the sawtooth collapse [29]. They have also been linked with fishbone activity [30].

The flattenings of the LIDAR temperature profiles around q = 1, observed in those cases, are likely to be associated with a helical m = 1, n = 1 mode. In the particular case of the partial sawtooth, some flat regions observed in the LIDAR profiles (and also with SXR and ECE data) correspond to an annular region. The MHD activity responsible for this annular region has decayed several milliseconds before the temperature profile has been measured.

In addition, depressions of the temperature located at the sawtooth inversion radius are seen after multiple pellet injection and are associated with 'snakes' [31]. The snake is a local density perturbation, normally located at the q = 1 surface, although it has also been found in JET at the q = 1.5 surface [32] and in W VII-A at the q = 2 surface [33]. This indicates that when the 'snake' is present, the plasma is in a helical equilibrium different from that normally found in JET plasmas.

An example of a flattening observed near the q = 1 radius after a sawtooth collapse is shown in Fig. 1. We will now discuss the example of a rotating m = 1, n = 1 mode that is apparently not associated with the sawtooth crashes. The case of a quasi-stationary m = 1 mode coupled to an m = 2 mode will be discussed in the next section.

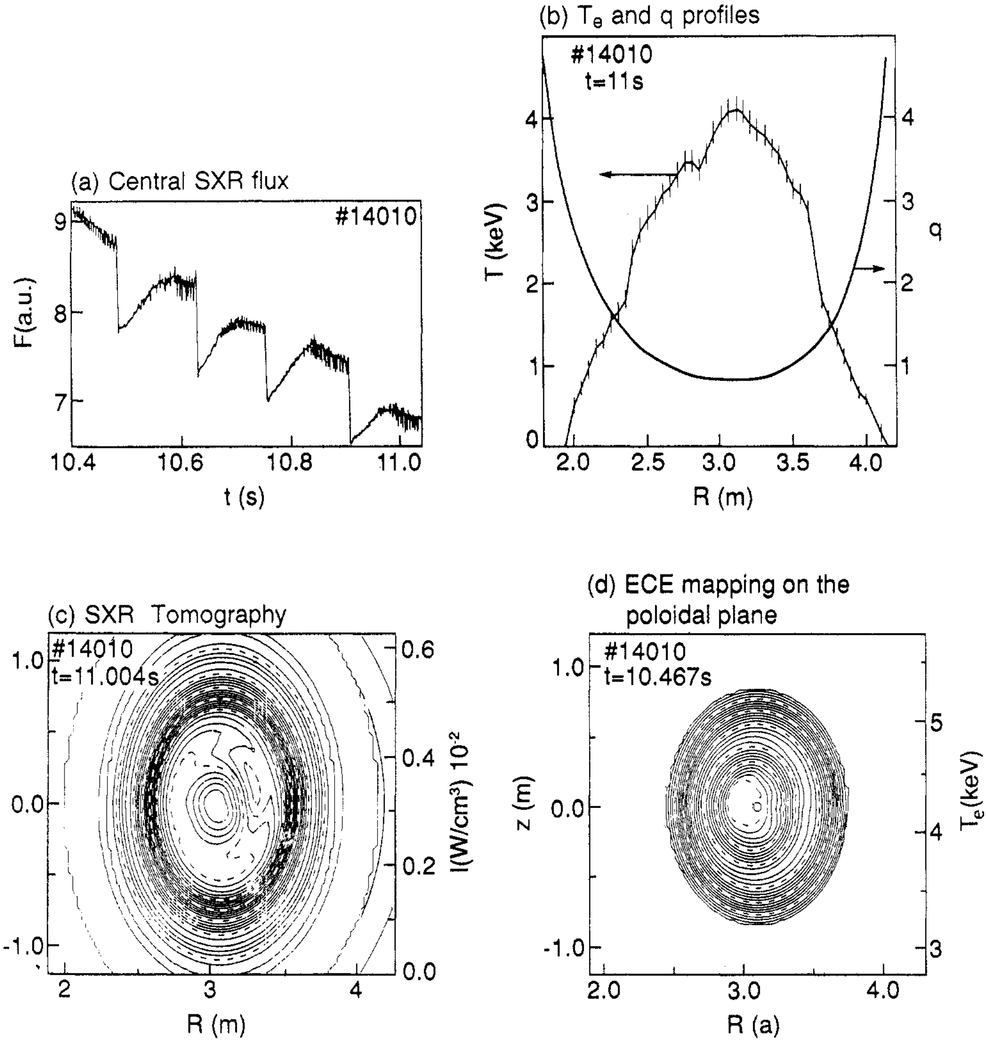

FIG. 3. Observations of a rotating m = 1, n = 1 mode. (a) Central SXR flux amplitude versus time, showing the evolution of a perturbation rotating at 400 Hz. (b) T_e and q profiles. (c) SXR tomography of the central plasma zone. (d) Mapping of ECE measurements on a poloidal cross-section. (N.B. SXR and ECE measurements with the required time resolution were not available for the same time. However, one can see from (a) that the central perturbations obtained in (c) and (d) can be associated with the same type of oscillation.)

In this example, a radiofrequency (RF) heated discharge (I_p = 3 MA, B_ϕ = 3.4 T, P_{RF} = 7 MW) shows oscillations, interpreted as continuous fishbone activity [30], with a nearly constant amplitude and frequency of 0.5 kHz both in SXR signals (Fig. 3(a)) and in ECE signals. These oscillations are observed before the sawtooth collapses, but their constant amplitude indicates that the sawtooth collapse is independent of them. (The MHD activity observed in this discharge is described in more detail in Ref. [30].)

Figure 3(b) shows the T_e and q profiles obtained. The large flat region close to the q = 1 surface indicates the presence of an m = 1 perturbation. From SXR measurements the toroidal mode number has been found to be n = 1. Phase reversals of the SXR signals indicate an m = 1 mode in the centre, with m = 2 and probably m = 3 modes at the outside, at the positions of rational q seen in Fig. 3(b). The reconstruction of the SXR midplane emission profile shows an m = 1 flattening coinciding with that of Fig. 3(b), while the SXR tomography of the central plasma zone (Fig. 3(c)) shows an m = 1 island related to the q = 1 surface. The mapping of the ECE signals for a full oscillation period on the poloidal plane (Fig. 3(d)) also shows an m = 1 perturbation at the position of q = 1. (The different phases of the m = 1 perturbation shown

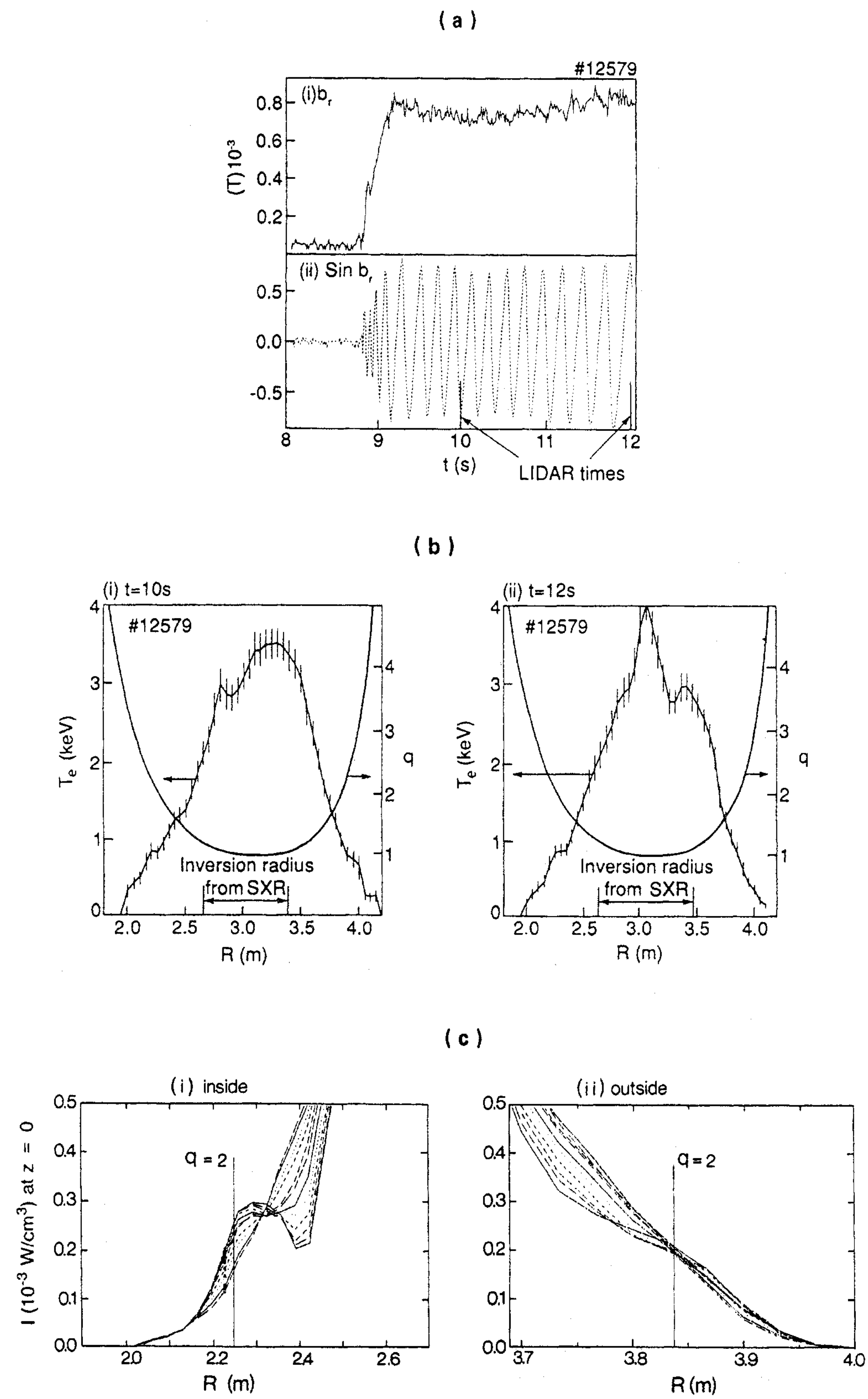

FIG. 4. Observations of a quasi-stationary $m = 2$, $n = 1$ mode. (a) Time traces of magnetic measurements showing: (i) the amplitude of the radial magnetic field perturbation b_r and (ii) the sine component of b_r.
(b) T_e and q profiles for two times: (i) $t = 10$ s and (ii) $t = 12$ s. (c) Radial structure of the SXR midplane emission profile for the $q = 2$ region showing: (i) the high field side and (ii) the low field side.

in the figures can be accounted for when we consider the mode rotation and the toroidal locations of the different diagnostics.)

2.3. Observation of m = 2, n = 1 modes

Large amplitude rotating or locked modes, usually with mode numbers (2, 1) or (3, 2), are observed under many operating conditions and may persist for many seconds. In particular, locked or quasi-stationary (slowly rotating) modes can appear early in the current rise, or after perturbations such as pellet injection or a large sawtooth collapse occurring after a period of sawtooth suppression [34]. Locked (2, 1) modes are also the main precursor for disruptions [14].

We discuss a quasi-stationary mode which appeared after a 'monster sawtooth' crash (I_p = 2 MA, B_ϕ = 2.1 T, P_{RF} = 4 MW). The signals from magnetic pick-up coils (Fig. 4(a)) show a slow oscillation of 4.25 Hz with a saturated amplitude. Magnetic data analysis indicated a dominant m = 2, n = 1 structure [35]. The same frequency was also measured with the different channels of the ECE and SXR diagnostics, suggesting a toroidal coupling [35] between external and central modes.

The T_e and q profiles obtained at two different times are shown in Fig. 4(b). As in the previous examples, an obvious flat region is seen in the T_e profiles close to q = 1 and the sawtooth inversion radii. Another large flat region is seen close to q = 2 on the inside of the profile taken at t = 12 s. In the earlier profile, at t = 10 s, the flatter structures close to q = 2 have widths inside the experimental error; however, their position, symmetry and temperature value, compared to the t = 12 s profile, indicate that they may be caused by an m = 2, n = 1 mode.

The magnetic signals show that between the two T_e profiles there is a 180° phase difference. The magnetic analysis provides the toroidal location where the O points of the n = 1 rotating islands are in the midplane, on the low field side. Thus, the poloidal location at the toroidal position (ϕ = 0°), where the instantaneous LIDAR measurements are made, can be obtained from the magnetic signals under the assumption of mode coupling of all n = 1 modes [36]. If we assume that the m = 2, n = 1 mode is coupled to a central m = 1, n = 1 mode, we find that the m = 1 perturbations on the two T_e profiles shown are in fact observed at the positions expected on opposite sides of the profiles [35].

SRX tomography confirms the existence of islands of low poloidal m numbers, m = 1 and m = 2, located at the identified rational q surfaces. Some activity is also seen around the q = 1.5 surface and is likely to be an m = 3, n = 2 mode. Figure 4(c) shows the reconstructed emission profiles around q = 2. It illustrates what is usually observed in the temperature profiles, that the radial extent of the perturbation is greater on the inner side. Because of this inside/outside asymmetry the perturbation may be only clearly visible on the inside. This can explain why the m = 2 mode is sometimes asymmetric on the LIDAR profiles. The figure also shows the rotation effect on the observed width, which is a maximum when the O point of the island is in full view.

The maximum width of the perturbation, observed on the inner side of the SXR emission profiles, is ~20 cm. The inner side of the LIDAR profile at t = 12 s shows a flattening around q = 2 with a width of 10–15 cm. The difference between the widths observed can be explained by a phase difference, since the LIDAR and SXR measurements are taken at different octants. Comparable widths are also estimated from the magnetic signals and from tearing mode calculations. From the amplitude of the m = 2, n = 1 oscillation measured in the magnetic signals, and assuming that the radial perturbed field varies with radius as $(r)^{m+1}$, one can estimate an island width of ~20 cm at the position where q = 2. From a numerical simulation of the tearing mode problem in the cylindrical approximation [25], where we used the experimental current density profile at t = 12 s, we calculated that the m = 2, n = 1 mode would saturate with an island width of ~17 cm.

2.4. Observation of m = 3, n = 2 modes

Modes with toroidal number n = 2 are also seen in many operating conditions, often already during the current rise phase. Enhanced n = 2 activity is measured at particular conditions, such as after pellet injection [37, 38] and after a 'monster sawtooth' collapse [24]. In some high β discharges the β collapse is associated with n = 2 and n = 3 activity [39].

The correlation between T_e perturbations at q = 1.5 and the observation of m = 3, n = 2 modes with other diagnostics is particularly clear in discharges with pellet injection. Examples have already been presented in the JET literature, so we will refer here to a pulse analysed in Ref. [38]. It showed that pellet injection during the current rise of limiter discharges is followed by a sharp increase in the n = 2 MHD activity. SXR analysis indicated a poloidal mode number of m = 3, while the emission profiles showed a flattened region around the q = 1.5 surface. Flatter regions at the same position were seen in the LIDAR temperature and pressure profiles.

It should be noted that in the data examined so far, the m = 3, n = 2 modes appear to affect the T_e profile to a similar extent as does the m = 2, n = 1 mode. The cylindrical approximation, however, predicts widths one order of magnitude smaller. Toroidal effects [40] may have to be invoked in order to explain the m = 3, n = 2 island widths suggested by the temperature profile observations.

3. SMOOTHER TEMPERATURE PROFILES

Smoother LIDAR T_e profiles are measured in some conditions where a reduction of MHD activity is

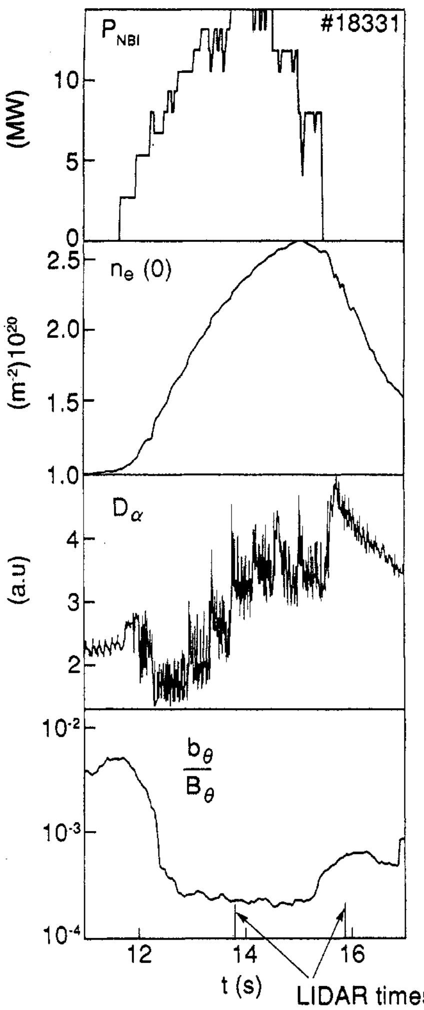

FIG. 5a. Time behaviour of plasma parameters during an H-mode: total additional power, central line density, D_α trace, showing ELMs and sawteeth, and ratio of the perturbed poloidal magnetic field (from an n = 1 combination of pick-up coil signals measured at 45° above the midplane on the lower field side) to the equilibrium poloidal magnetic field.

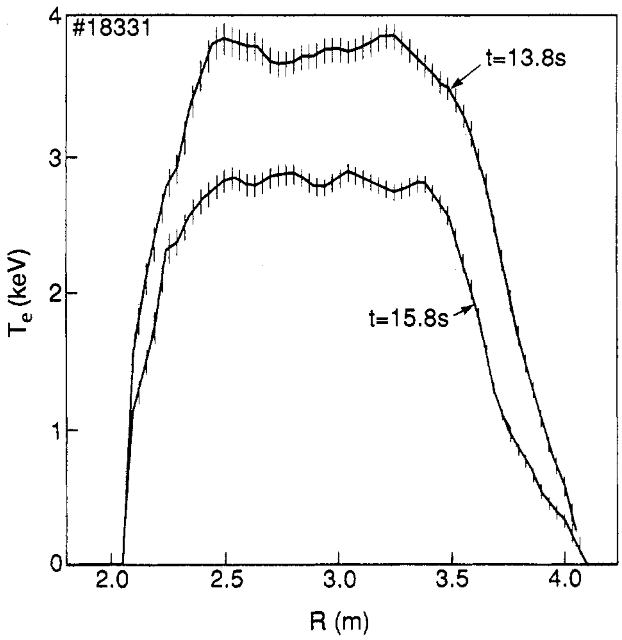

FIG. 5b. Electron temperature profiles.

observed. Most noticeable are the smooth central regions after pellet injection and the smooth outer regions after an L–H transition. A lack of large profile structures has also been observed during periods of sawtooth stabilization. Part of this effect is certainly also due to a better photon statistic caused by the higher electron density in pellet fuelled and H-mode discharges. However, error bars are taken into account in our analysis.

3.1. Discharges with pellet fuelling

Pellet injection in the current rise phase of limiter discharges has the effect of keeping q_0 above unity and consequently delaying the appearance of sawtooth activity [38]. After pellet injection, the T_e profiles show smooth central regions, in agreement with the absence of m = 1, n = 1 modes.

3.2. Discharges with the H-mode

Smooth LIDAR T_e profiles are observed during the H-phase [41] of some JET discharges where the L–H transition is followed by a decrease of MHD activity. In these cases, the T_e profiles still show central perturbations around q = 1, as one would expect, since usually sawtooth activity is not suppressed, but the profiles are very smooth in the outer regions, indicating a reduction of internal modes with m > 1.

To illustrate this, Fig. 5 shows an H-mode dominated by edge localized modes (ELMs), where the n = 1 activity measured with the magnetic pick-up coils is decreased by a factor of ten. The LIDAR T_e profiles show smooth outer regions. (In this particular example the T_e profiles were available soon aftersawtooth crashes and therefore are flat in the central region.)

However, not all H-modes are accompanied by a decrease in MHD activity. Clear counter-examples are H-regimes occurring for values of the toroidal β parameter close to the Troyon limit, which show large amplitude n = 1 modes such as fishbones and sometimes enhanced n = 2 and n = 3 activity [39]. As in the examples in the previous section, the T_e profiles show large structures that can be correlated with perturbations observed in SXR and ECE signals.

3.3. Discharges with 'monster sawteeth'

Sawtooth stabilization with $q_0 < 1$ is obtained in JET, with high power additional heating, for periods lasting up to 5 s. The level of coherent MHD modes is low, as reported in Ref. [24], and is of the order of $\delta B_\theta/B_\theta \leq 10^{-4}$.

As a general trend, the LIDAR temperature profiles obtained during the temperature saturation phase of sawtooth free periods do not show large perturbations, but exceptions do occur, as is the case for the early phase of the 'monster sawtooth' shown in Fig. 2. Some exceptions may also be explained by the presence of fishbones, which have been observed occasionally during 'monster sawteeth' [30].

4. STATISTICAL COMPARISON WITH RESULTS OF EQUILIBRIUM ANALYSIS

To investigate the correlation between the q profiles and the perturbations in the T_e profiles, a numerical method was used to analyse statistically the complete set of 1988 LIDAR data. A movable grid was used to sample the local slope of the temperature profile. A selection criterion was used which records an observation when the change in gradient is outside the temperature profile error bars. The R co-ordinates of the points of minimum slope thus obtained are recorded. The radial positions of the reduced slope steps on the LIDAR profiles were compared with the positions of the rational q surfaces. This comparison is shown in contour plots in the (q, R) plane, which represent the percentage of coincidence of the rational q surfaces with the LIDAR profile steps, at any given radius R.

Figure 6 shows the contour plots obtained for the most reliable data (in LIDAR profiles characterized by

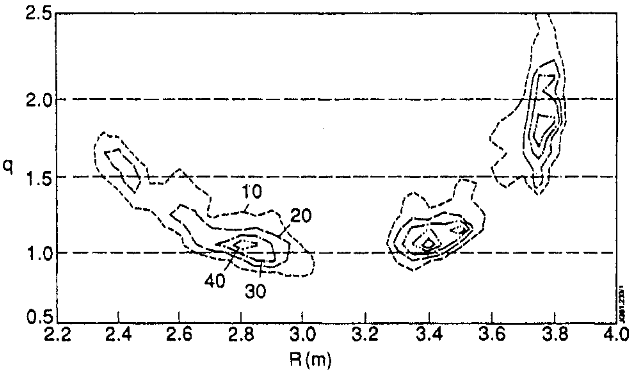

FIG. 6. Contour plots of the frequency of coincidence of 'bumps' on the T_e profiles, with q values at any given R, for a grid cell size $\Delta q \times \Delta R = 0.1 \times 0.05$ cm. The number of observations is 1785 on the outside and 1585 on the inside; the maximum frequency is 58. The contour lines start at 10 and increase at intervals of 10. Because of problems with stray light that may occur at $R < 2.25$ m, a smaller number of observations was found around q = 2 at the high field side.

the error $\delta T_e/T_e < 0.2$ everywhere and in q profiles characterized by the systematic consistency checks on the magnetic data being satisfied [20]). Note the correlation of the observations with discrete values of q occurring around q = 1, q = 3/2 and q = 2 when allowing for the spatial resolution of the LIDAR system of 0.09 m and the uncertainty of the central q values. A higher number of q = 2 plateaus was found on the outside because of inner wall stray light problems. Most of the profiles in the database were measured during the plasma current flat-top phase when the q profiles of JET discharges are very similar and very steep on the low field side owing to the aspect ratio. This explains the small spread in radius observed in the figure. (Electronic tests designed to check whether the bunching of the data in R could be an artefact of the LIDAR system are described in the Appendix.)

The statistical analysis confirms that the presence of flat T_e regions at rational values of q on both the inside and the outside of the profile is not a random event. The correlation between the occurrence of flat regions near q = 1 and q = 2, on the inside and outside of T_e profiles, was studied. As expected from the symmetry of MHD perturbations, the observed q = 1 plateaus on the inside and the outside are not correlated, while the observed q = 2 plateaus, appearing simultaneously on both sides, are correlated. A further result was that q = 1/q = 2 flattenings on the inside/outside were anti-correlated with the observed q = 2/q = 1 flattenings on the outside/inside. This can be explained by the well known phase coupling of the (1, 1) and (2, 1) modes in tokamaks [36].

5. SUMMARY

Comparison between typical LIDAR T_e profiles in the equatorial plane of JET and the q profiles determined from magnetic equilibrium calculations shows that the locations of flatter regions of T_e are correlated with rational values of q. The existence of perturbations located at the rational surfaces of q is further confirmed by SXR, ECE and magnetic data analysis. In most cases studied, the flattenings in T_e can be associated with the observation of magnetic islands, the most important having mode numbers (1, 1), (2, 1) and (3, 2).

Flat regions of T_e are seen in most modes of JET operation and can be correlated with many types of MHD events. For example, quasi-stationary modes may appear early in the current rise phase and remain throughout the discharge, the flat regions of T_e having a behaviour consistent with that of magnetic islands caused by nearly saturated resistive modes. Conversely, when MHD activity is suppressed, the LIDAR T_e profiles are seen to be smoother, for example when sawtooth activity has been suppressed during 'monster sawteeth' or after pellet injection.

The statistical analysis shows that the simultaneous appearance of flat regions at $q = 2$ on the inside and the outside of a T_e profile is not a random event. However, consistent with the fact that in toroidal geometry with large Shafranov shift the X and O points of an island are not poloidally equidistant [26], the flattening of modes with even parity is sometimes seen only on one side of the T_e profile in the equatorial plane. Naturally, this also occurs for odd parity, and it was confirmed to be the case for most perturbations around $q = 1$. Further, the statistical analysis shows that the observation of a $q = 1$ plateau on the inside of the temperature profile is anti-correlated with the observation of a $q = 2$ plateau on the outside. This implies a phase relation between the modes which may be explained by mode coupling.

It is generally observed that the LIDAR T_e plateaus are wider on the high field side. This is consistent with the SXR emission data and the magnetic analysis with the FAR code [28] for a toroidal JET plasma. The width of the T_e flattenings is consistent with the size of perturbations measured with other diagnostics. It should be noted that in the data examined so far, the $m = 3$, $n = 2$ mode appears to affect the T_e profile to a similar extent as does the $m = 2$, $n = 1$ mode.

In summary, we have shown a significant correlation between perturbations in the temperature profile data and the modes determined from analyses of independent experimental measurements. These temperature profile perturbations occur in most discharges, under all kinds of plasma conditions.

Appendix

The LIDAR diagnostic uses a time of flight technique to infer spatial profiles from time varying signals. Thus, electronic ringing in the detector signals for the different spatial channels could lead to deviations from a smooth profile, and, if present, this would occur more frequently at certain radii than at others. Since the majority of JET discharges show spatial q profiles located inside a certain band, the bunching of observations in the R domain would also lead to bunching in the q domain. To investigate this problem, a test experiment was carried out to illuminate the photodetectors with an optical square pulse. The 350 ps duration ruby laser pulse, normally used for Thomson scattering, was passed through open air over a distance of 2.5 m, about 6 m away from the detector. Both Mie scattering from dust particles and Rayleigh scattering from air contribute to the observed scattering signal. No ringing with the characteristic frequency close to that corresponding to the observed spatial bunching at 3.8, 3.4, 2.8 and 2.4 m was found on the fast rise signal.

The spatial resolution of the diagnostic, determined by the combination of the laser pulse duration and the response time of the detection system, was improved to about 9 cm by using a signal deconvolution technique. A confidence check on this fast converging numerical procedure was carried out by comparing its results with those from a commercially available (but slow) maximum entropy deconvolution software package. The results were in complete agreement.

ACKNOWLEDGEMENTS

The authors wish to thank Dr. R. Galvão for useful comments, Dr. D. Campbell and the ECE group for assistance with ECE data, Mr. C. Gowers for the many discussions and help with the LIDAR data and Dr. D. Ward for help with the analysis of magnetic data.

REFERENCES

[1] WHITE, R., MONTICELLO, D.A., ROSENBLUTH, M., WADDELL, B.V., Phys. Fluids **20** (1978) 800.

[2] BATEMAN, G., MORRIS, R.N., Phys. Fluids **29** (1986) 753.

[3] BHATTACHARJEE, A., GLASSER, A.H., AVINASH (Khare), SEDLAK, J.E., Phys. Fluids **29** (1986) 242.
[4] SAUTHOFF, N.R., VON GOELER, S., STODIEK, W., Nucl. Fusion **18** (1978) 1445.
[5] W VII-A Team, in Plasma Physics and Controlled Nuclear Fusion Research 1980 (Proc. 8th Int. Conf. Brussels, 1980), Vol.1, IAEA, Vienna (1981) 173.
[6] JAENICKE, R., and W VII-A Team, Nucl. Fusion **28** (1988) 1737.
[7] TSUJI, S., NAGAYAMA, Y., KAWAHATA, K., NODA, N., TANAHASHI, S., Nucl. Fusion **22** (1982) 1082.
[8] SMEULDERS, P., A Fast Plasma Tomography Routine with Second-Order Accuracy and Compensation for Spatial Resolution, Rep. IPP-2/252, Max-Planck-Institut für Plasmaphysik, Garching (1983).
[9] PARDO, C., ZURRO, B., and TJ-I Team, in Controlled Fusion and Plasma Heating (Proc. 13th Eur. Conf. Schliersee, 1986), Vol. 10C, Part I, European Physical Society (1986) 117.
[10] GRANETZ, R.S., SMEULDERS, P., Nucl. Fusion **28** (1988) 457.
[11] WESTERHOF, E., SMEULDERS, P., LOPEZ CARDOZO, N.J., Nucl. Fusion **29** (1989) 1056.
[12] SALMON, N.A., BARTLETT, D.V., COSTLEY, A.E., HUGON, M., in Controlled Fusion and Plasma Physics (Proc. 14th Eur. Conf. Madrid, 1987), Vol. 11D, Part III, European Physical Society (1987) 1248.
[13] SNIPES, J.A., CAMPBELL, D.J., HAYNES, P.S., et al., Nucl. Fusion **28** (1988) 1085.
[14] WESSON, J.A., GILL, R.D., HUGON, M., et al., Nucl. Fusion **29** (1989) 641.
[15] SALZMANN, H., HIRSCH, K., NIELSEN, P., et al., Nucl. Fusion **27** (1987) 1925.
[16] SALZMANN, H., BUNDGAARD, J., GADD, A., et al., Rev. Sci. Instrum. **59** (1988) 1451.
[17] NAVE, M.F.F., LAZZARO, E., GOWERS, C., et al., in Controlled Fusion and Plasma Heating (Proc. 15th Eur. Conf. Dubrovnik, 1988), Vol. 12B, Part I, European Physical Society (1989) 441.
[18] BLUM, J., GILBERT, J.C., Le FOLL, J.L., THOORIS, B., in Computational Physics (Proc. 8th Eur. Conf. Bad Eibsee, 1986), Vol. 10D, European Physical Society (1986) 49.
[19] LAZZARO, E., MANTICA, P., Plasma Phys. Control. Fusion **30** (1988) 1735.
[20] BLUM, J., LAZZARO, E., O'ROURKE, J., et al., Nucl. Fusion **30** (1990) 1475.
[21] LAO, L.L., FERRON, J.R., GRÖBNER, R.J., et al., Nucl. Fusion **30** (1990) 1035.
[22] VABISCHEVICH, P.N., ZOTOV, I.V., Sov. J. Plasma Phys. **14** (1988) 759.
[23] STOTT, P.E., "Review of JET diagnostics and results", Basic and Advanced Fusion Plasma Diagnostic Techniques (Proc. Course and Workshop Varenna, 1986), Vol. 3, CEC, Brussels (1987) 845.
[24] CAMPBELL, D.J., START, D.F.H., WESSON, J.A., et al., Phys. Rev. Lett. **60** (1988) 2148.
[25] WESSON, J.A., Nucl. Fusion **18** (1978) 87.
[26] FUSSMANN, G., GREEN, B.J., ZEHRFELD, H.P., in Plasma Physics and Controlled Nuclear Fusion Research 1980 (Proc. 8th Int. Conf. Brussels, 1980), Vol.1, IAEA, Vienna (1981) 353.
[27] HENDER, T.C., ROBINSON, D.C., SNIPES, J.A., in Plasma Physics and Controlled Nuclear Fusion Research 1986 (Proc. 11th Int. Conf. Kyoto, 1986), Vol.1, IAEA, Vienna (1987) 291.
[28] CHARLTON, L.A., HOLMES, J.A., LYNCH, V.A., et al., J. Comput. Phys. **68** (1990) 270.
[29] CAMPBELL, D.J., EDWARDS, A.W., PEARSON, D., in Controlled Fusion and Plasma Physics (Proc. 16th Eur. Conf. Venice, 1989), Vol. 13B, Part II, European Physical Society (1989) 509.
[30] NAVE, M.F.F., CAMPBELL, D.J., JOFFRIN, E., et al., Nucl. Fusion **31** (1991) 697.
[31] EDWARDS, A.W., CAMPBELL, D., CHEETHAM, A., et al., in Controlled Fusion and Plasma Heating (Proc. 15th Eur. Conf. Dubrovnik, 1988), Vol. 12B, Part I, European Physical Society (1988) 342.
[32] WELLER, A., CHEETHAM, A.D., EDWARDS, A., et al., Phys. Rev. Lett. **59** (1987) 2303.
[33] WELLER, A., BRAKEL, R., BURHENN, R., et al., in Controlled Fusion and Plasma Heating (Proc. 17th Eur. Conf. Amsterdam, 1990), Vol. 14B, Part II, European Physical Society (1990) 479.
[34] SNIPES, J.A., CAMPBELL, D.J., HENDER, T.C., HELLERMANN, M. von, WEISEN, H., Nucl. Fusion **30** (1990) 205.
[35] SNIPES, J.A., CAMPBELL, D.J., HUGON, M., et al., in Controlled Fusion and Plasma Heating (Proc. 15th Eur. Conf. Dubrovnik, 1988), Vol. 12B, Part I, European Physical Society (1988) 346.
[36] KARGER, F., LACKNER, K., FUSSMANN, G., et al., in Plasma Physics and Controlled Nuclear Fusion Research 1976 (Proc. 6th Int. Conf. Berchtesgaden, 1976), Vol.1, IAEA, Vienna (1977) 267.
[37] JET Team, in Plasma Physics and Controlled Nuclear Fusion Research 1988 (Proc. 12th Int. Conf. Nice, 1988), Vol.1, IAEA, Vienna (1989) 215.
[38] HUYSMANS, G.T., GALVÃO, R.M.O., GOEDBLOED, J.P., LAZZARO, E., SMEULDERS, P., Plasma Phys. Control. Fusion **31** (1989) 2101.
[39] SMEULDERS, P., ADAMS, J.M., BALET, B., et al, in Controlled Fusion and Plasma Heating (Proc. 17th Eur. Conf. Amsterdam, 1990), Vol. 14B, Part I, European Physical Society (1990) 323.
[40] EDERY, D., PELLAT, R., SOULE, J.L., A Consistent Three Dimensional Model for the Non-Linear Evolution of the Resistive Tearing Modes in Toroidal Plasmas, Rep. EUR-CEA-FC-1109, Association Euratom-CEA, Département de recherches sur la fusion contrôlée (1981).
[41] BALET, B., BOYD, D., CAMPBELL, D.J., et al., High Temperature L and H Mode Confinement in JET, Rep. JET-P(89)81, JET Joint Undertaking, Abingdon, Oxfordshire (1989).

(Manuscript received 27 December 1990
Final manuscript received 24 January 1992)